Spall in Aluminium with Helium Bubbles under Laser Shock Loading *

Da-Wu Xiao(肖大武)[1**], Li-Feng He(何立峰)[1], Ping Zhou(周萍)[1], Dong-Li Zou(邹东利)[1], Hua Shu(舒桦)[2]

[1]*Institute of Materials, China Academy of Engineering Physics, Mianyang 621700*

[2]*Institute of Laser, China Academy of Engineering Physics, Mianyang 621700*

(Received 2 December 2016)

The spallation behaviors of Al+0.2 wt% ^{10}B targets and neutron irradiated Al+0.2 wt% ^{10}B targets with 5 nm radius helium bubble subjected to direct laser ablation are presented. It is found that the spall strength increases significantly with the tensile strain rate, and the helium bubble or boron inclusions in aluminum reduces the spall strength of materials by 34%. However, slight difference is observed in the spall strength of unirradiated samples compared with the irradiated sample with helium bubbles.

PACS: 62.50.−p, 62.50.Ef, 62.20.mm DOI: 10.1088/0256-307X/34/5/056201

Defects such as cracks or voids have significant influences on the deformation and damage behavior of materials, especially void nucleation and growth coupled with plasticity are responsible for shock-induced spallation damage.[1−3] As a typical harmful defect, the creation of helium atoms is one of the general or most important damage mechanisms for metals used in fusion reactor or nuclear power technology. For investigation of the mechanical properties of metals with bubbles, an approximately uniform distribution of the bubbles in the bulk of the target is required. In most previous studies, samples with helium bubbles are mainly accomplished by tritium decay techniques[4] or helium implantation in near surface.[5,6] Helium atoms will accumulate in the lattice because they are not dissolved in the material matrix, the accumulated helium atoms precipitate and gather each other to form a helium bubble, which causes metal parts to occur premature intercrystalline fracture. Early researches showed that helium bubbles can cause significant deterioration of the mechanical response of materials under static loading conditions, especially in plasticity and fracture properties. At higher temperatures or under external tensile stress, helium bubbles possibly grow at grain boundaries, phase boundaries, and dislocations, leading to drastic embrittlement. Research under dynamic loading conditions is quite rare. Kubota *et al.*[7] and Shao *et al.*[8] calculated the dynamic strength of aluminum containing an initial distribution of microscopic defects and nanometric bubbles. Raicher *et al.*[9] investigated the equation of state (EOS) for aluminum with helium bubbles with the molecular dynamics method. Gas gun experiments on Al-^{10}B samples reported by Glam *et al.* indicated that the presence of helium bubbles and ^{10}B in materials will decrease the spall strength obviously.[10,11] In this work, helium in metals is induced by a method of neutron irradiation of Al-^{10}B samples.[10] Shock waves are generated in neutron irradiated Al-^{10}B targets containing helium bubbles and unirradiated Al-^{10}B targets by direct laser ablation loading to obtain the results under much higher pressure and strain rates than those of gas gun experiments. An additionally interesting aspect of the present experiments on aluminum targets is that the ratio of the grain size to the sample thickness is approximately unity. These experiments may be helpful to resolve the problem what will arise when shock wave experiments are scaled to sub-millimeter dimensions.

The Al-^{10}B samples were prepared by melting pure aluminum (99.9999%) with 0.2 wt% boron powder (purity>99.9%, ^{10}B abundance 96%) in an arc furnace at 1200℃ for 0.5 h. After solidification the Al-^{10}B alloy was neutron irradiated in the nuclear reactor with 10 MW power for 132 h, in which the accumulated illumination of thermal neutron I is 2.37×10^{23} n/m^2. The concentration of He atoms, $n_{\rm He}$, produced in the bulk samples from the reaction ^{10}B+n→^{7}Li+^{4}He is given as $n_{\rm He} = I\sigma N_{\rm B}$, where $\sigma = 4.0\times10^{-25}$ m^2 is the cross section of the ^{10}B atom, and $N_{\rm B}$ is the number of ^{10}B atoms per unit volume. The atom densities of He and B, which are 3.1×10^{25} m^{-3} and 3.24×10^{26} m^{-3}, respectively, can be calculated with 0.2 wt% ^{10}B average concentration for the post-irradiated sample. After irradiation, the sample was cut into small pieces and φ3 mm×0.15 mm samples were prepared for the laser impact experiments. To obtain helium bubbles, the sample was heated with a duration of 1 h at a temperature of 500℃. Transmission electron microscopy measurements revealed that the average bubble radius is about 5 nm. Shock wave experiments were performed by direct laser ablation loading on three distinct targets: (1) pure Al, (2) Al+0.2 wt% ^{10}B, and (3) Al+0.2 wt% ^{10}B with helium bubbles, using the Shenguang-Ⅱ Nd:glass laser (converted to $\lambda = 0.351$ μm) of the National Laboratory on High Power Laser and Physics. In this experiment, the drive laser was converted to the third harmonic (3ω) and directly illuminated the target. The laser beam was

*Supported by the Science Foundation of China Academy of Engineering Physics under Grant No 9090702.

**Corresponding author. Email: hopkinson@163.com

© 2017 Chinese Physical Society and IOP Publishing Ltd

smoothed using a lens-array system to eliminate large-scale spatial modulation and to obtain a flat-topped profile in the focal plane. The temporal profile of the laser is nearly square with a full width at half maximum of ∼3 ns and a rise and fall time of ∼300 ps. The absorbed laser intensity of the focal spot was $\sim 10^{11}$ W/cm^2 with a flat region of 2.6 mm×3.7 mm. To monitor the process of the spall fracture, time-resolved free surface velocity profiles of the shocked sample were measured with a line VISAR. The VISAR system had a temporal resolution of ∼20 ps and a spatial resolution of ∼7 μm. The density of the samples ρ_0 (2699±0005 g/cm^3) was measured using the Archimedes technique, both the longitudinal speeds of sound C_0 (654±003 km/s) and the bulk speed of sound C_b (545±003 km/s) were obtained by the resonant ultrasound spectroscopy (RUS) technique. The Hugoniot elastic limit (HEL) and spall strength were calculated and analyzed from the free surface velocity measurements.

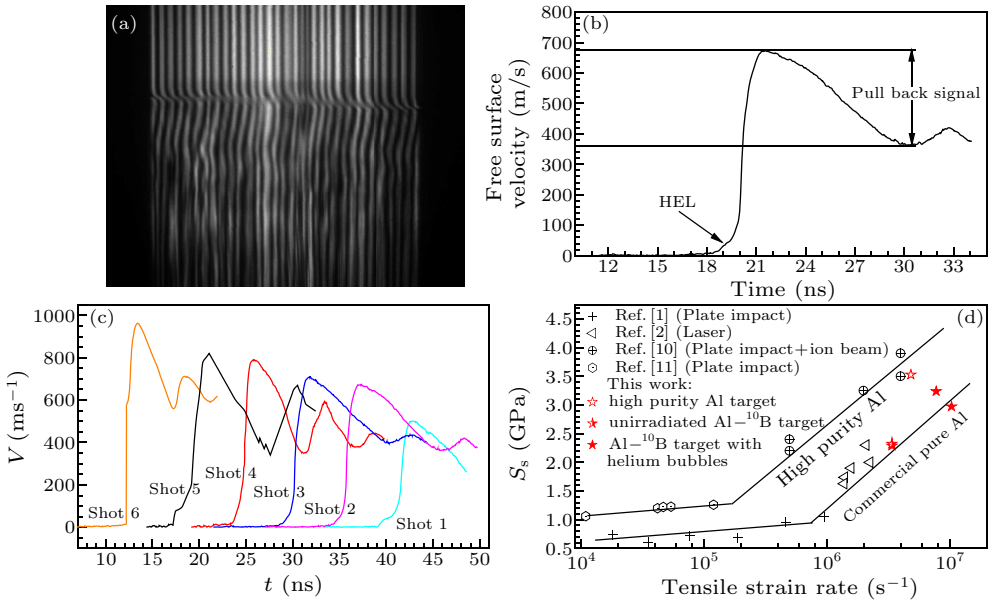

Fig. 1. Experimental results of Al and Al-^{10}B targets by direct laser ablation: (a) typical line VISAR diagnostics, (b) subsequent velocity-time response of the Al-^{10}B target with drive laser energy of 41 J, (c) all of the free surface velocity profiles, and (d) spall strength of Al as a function of the tensile strain rate.

Typical line VISAR image of the experiment is shown in Fig. 1(a) (the drive laser energy is about 41 J at 3 ω). Distance is represented in the horizontal direction of the image, with the time in the vertical direction. The temporal scale of the image is 50 ns. The length of the etalon is 60 mm corresponding to the fringe constant of 900 m/s/fringe. Figure 1(b) shows the free surface velocity profile of the experiment. Clearly labeled in this figure are the HEL of the material, as well as the pullback signal associated with the difference between the maximum and minimum velocities. Based on the recorded velocity history, the HEL value $\sigma_{\rm hel}$ can be determined by

$$\sigma_{\rm hel} = \rho_0 C_0 u_{\rm hel}/2, \tag{1}$$

where ρ_0 is the density of the samples, C_0 is the longitudinal speed of sound, and $u_{\rm hel}$ is the velocity at the elastic-plastic transition. The 'pull-back' signal in free surface velocity is related to the material dynamic spallation. The spall strength $\sigma_{\rm s}$ could be estimated by

$$\sigma_{\rm s} = \rho_0 C_{\rm b} \Delta u/2, \tag{2}$$

where $C_{\rm b}$ is the bulk speed of sound, and Δu is the pullback value. Free surface velocity histories of all the six targets with different initial microstructures are shown in Fig. 1(c). Shots 1–6 represent the targets number. Shot 1 is a high purity aluminum (99.9999%) target, shots 2 and 3 are unirradiated Al+0.2 wt% ^{10}B targets, and shots 4–6 are Al+0.2 wt% ^{10}B with helium bubble targets. The corresponding laser incident intensities are 0.39 × 10^{12} W/cm^2, 0.17 × 10^{12} W/cm^2, 0.34 × 10^{12} W/cm^2, 0.28 × 10^{12} W/cm^2, 0.47 × 10^{12} W/cm^2, and 1.6 × 10^{12} W/cm^2, respectively. The targets will experience different damage evolution processes up to complete spall with the variation of the laser incident density: (1) no spall for shot 2, (2) incipient spall for shots 3 and 4, and (3) complete spall for shots 1, 5 and 6. Based on the free surface velocity profiles, $\sigma_{\rm hel}$ and $\sigma_{\rm s}$ were calculated using Eqs. (1) and (2). The values of $\sigma_{\rm hel}$ for shots 1–5 are 0.69 GPa, 0.30 GPa, 0.41 GPa, 0.38 GPa and 0.84 GPa, and the values of $\sigma_{\rm s}$ for shots 1, 3–6 are 3.53 GPa, 2.32 GPa, 2.29 GPa, 3.24 GPa and 2.97 GPa, respectively. The tensile strain rate of spall was estimated by the unloading part of the incident shock pulse. The measured spall strength from this study is plotted as a function of the tensile strain rate in Fig. 1(d), together with other reports of high purity

aluminum (Al HP) and commercial pure aluminum (Al CP) for comparison.[12,13,14] One can notice that an apparent increase of the spall strength with the tensile strain rate is evidenced for both Al-^{10}B targets and Al-^{10}B targets with helium bubble compared with other Al CP results, and the spall strength is lower than that of Al HP under similar loading conditions. The addition of 0.2% ^{10}B in pure aluminum reduces the spall strength of the material by about 34% under the laser shock condition, which is consistent with the findings of Glam *et al.*,[11] who investigated the influence of the helium on the spall strength in aluminum by plate impact with a gas gun.

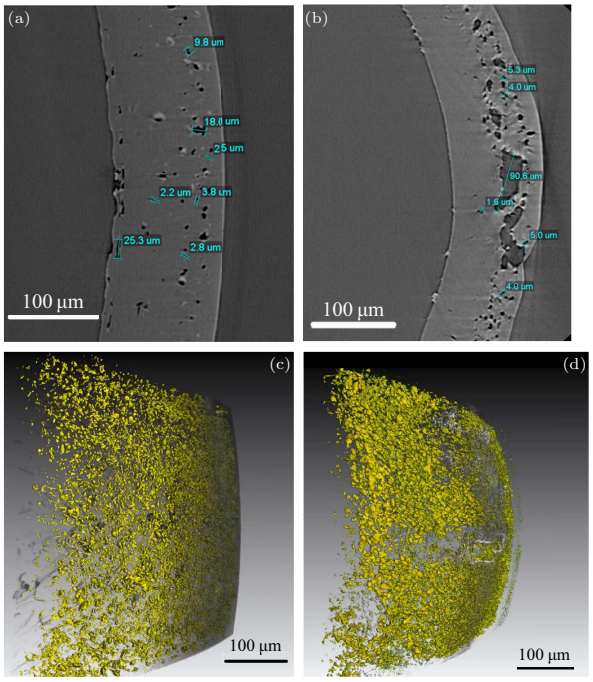

Fig. 2. X-ray tomography results of Al-^{10}B targets without helium bubbles: (a) no spall, (b) incipient spall, (c) 3D visualisation of the porosity for shot 2, and (d) 3D visualisation of the porosity for shot 3.

The shape distribution of spall damage is easily discerned qualitatively from inspecting the 3D x-ray microscopy for each material condition with an Xradia Versa 520 machine. Figure 2 illustrates a comparison of the characteristics of pores in recovery targets of shots 2 and 3. The spall signal has not been observed in the free surface velocity profile of shot 2, while an apparent spall signal was recorded for shot 3. The 2D slices of cross section of the impacted plane in target are shown in Figs. 2(a) and 2(b). It can be seen that there are only a few numbers of pores that can be detected in the recovery sample of shot 2. The size of most of the microvoids is below 20 μm, and the voids keep isolated in the target, and did not coalesce with each other. With a higher laser incident intensity, the number of voids in the recovery sample of shot 3 are dramatically denser than that of shot 2, and the voids evolve into large flat voids with a largest length of about 90 μm. Also, the distribution of voids in this case was relatively concentrated at this location near the free surface of the sample. Figures 2(c) and 2(d) show the 3D visualizations of the pores detected inside the sample. It should be noted that under the as-built condition, the recovery sample of shot 3 has been shown to contain a greater number density of pores in comparison with that seen in shot 2, where the volume fraction of pores in that case reveals a clear shape change from predominately fine and uniform voids for shot 2 to large flat voids for shot 3. In Fig. 3, pore volumes have been plotted against their numbers for all the pores detected within the as-built sample. Detailed analysis has confirmed that all the pores appearing during the spall damage stages can be correlated to the growth of pores. From this analysis, it is immediately apparent that such pores (Fig. 3(a)) have coalesced, which evolves into the incipient spall (Fig. 3(b)).

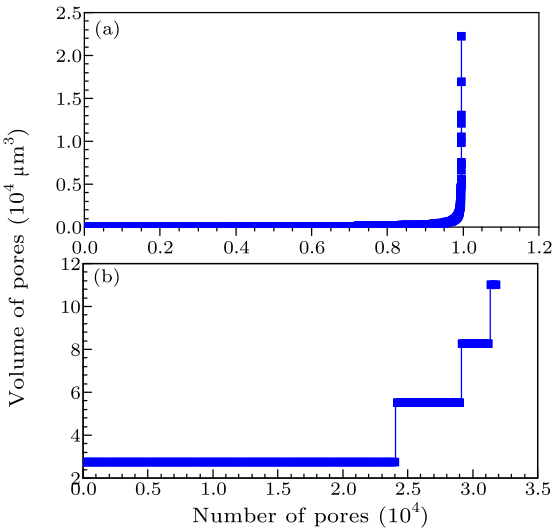

Fig. 3. Quantification of all the pores detected within the as-built targets: (a) shot 2 and (b) shot 3.

Optical micrographs of the grains size distribution of the un-impacted Al HP and un-impacted Al-^{10}B targets are presented in Figs. 4(a) and 4(b). Most of the pure aluminum grains are 20–100 μm, while most of the Al-^{10}B grains are 280–600 μm for long-duration heat treatment at high temperatures, with a few acicular AlB_2 impurities distributing inside grains. Generally, materials with higher grain size provide better resistance to spall fracture because they contain less grain boundaries that can be potential microvoid nucleation sites, and the impurities are known to reduce the spall strength.[15,16] For our experiments, the AlB_2 impurities probably play a more important role than the grain size for the spall fracture evolution in the aluminum material. For the Al HP target, most voids and cracks preferred to nucleate along the grain boundary, while the impurities seem to be preferred sites for void growth in the Al-^{10}B target, which cau-

ses the decrease of the spall strength. In the experiments of Al-^{10}B targets, with or without bubbles (shots 3 and 4), the average measured pullback velocity is $\Delta u = 313 \pm 2\,(\mathrm{m/s})$ and the calculated one is 2.30±0.02 GPa. These findings reveal that the presence of a helium bubble in the aluminum does not seem to affect the aluminum response to shock compression, which also implies that the spall strength of aluminum is controlled more by the rate of void nucleation rather than its growth under laser shock loading. The loading pulse of laser shock is shorter and the corresponding strain rate is much higher in comparison with the gas gun, the voids or cracks do not have enough time to coalesce and grow up before the 'pull-back' signal reflected in the free surface, and the helium bubble play a principal role in the pinning effect of voids or crack growth rather than the void nucleation.

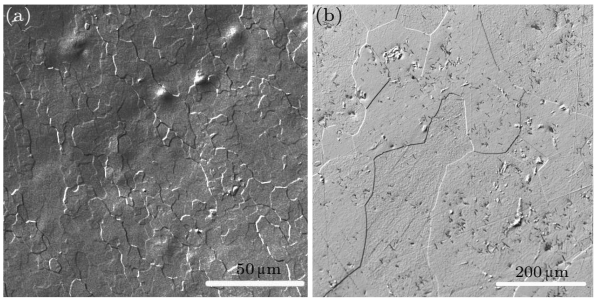

Fig. 4. Optical micrograph of the un-impacted Al targets: (a) high purity Al and (b) Al-^{10}B.

In summary, it has been conclusively demonstrated that the helium bubbles or boron inclusions can cause an obvious decrease in the spall strength in the aluminium under direct laser impact loading. Using a non-destructive x-ray CT, the pores in recovered targets have been tracked, confirming that the spall strength of Al is determined more by the rate of void nucleation rather than its growth under laser shock loading. The comparison results of high purity Al, unirradiated Al+0.2 wt% ^{10}B targets and Al+0.2 wt% ^{10}B target with 5 nm radius helium bubbles indicating that the impurities rather than grain size or helium bubble significantly influenced the spall strength, also revealing that the helium bubbles play a principal role in the pinning effect of voids or cracks growth rather than the void nucleation.

We gratefully acknowledge the valuable support for the experiments by the Shenguang-Ⅱ technical crews.

References

[1] Chen X, Asay J R, Dwivedi S K and Field D P 2006 *J. Appl. Phys.* **99** 023528
[2] Wang Y, He H, Qi M, Shen L and Bai B 2007 *J. Appl. Phys.* **102** 073518
[3] Wang Y, Qi M, He H and Wang L 2014 *Mech. Mater.* **69** 270
[4] Satou M, Koide H, Hasegawa A, Abe K, Kayano H and Matsui H 1996 *J. Nucl. Mater.* **233** 447
[5] Moreno D and Eliezer D 1996 *Scrip. Mater.* **35** 1385
[6] Marian J, Wirth B D and Perlado M 2002 *Phys. Rev. Lett.* **88** 255507
[7] Kubota A, Reisman D B and Wolfer W G 2006 *Appl. Phys. Lett.* **88** 241924
[8] Shao J L, Wang P and He A M 2014 *J. Appl. Phys.* **116** 111
[9] Raicher E, Glam B, Henis Z, Pecker S, Eliezer S and Moreno D 2009 *J. Appl. Phys.* **106** 083519
[10] Glam B, Eliezer S, Moreno D and Eliezer D 2009 *J. Nucl. Mater.* **392** 413
[11] Glam B, Eliezer S, Moreno D, Eliezer D, Perelmutter L, Sudai M and Eliezer D 2010 *Int. J. Fract.* **163** 217
[12] Glam B, Strauss M, Eliezer D and Moreno D 2014 *Int. J. Impt. Eng.* **65** 1
[13] Kanel G I, Razorenov S V, Baumung K and Singer J 2001 *J. Appl. Phys.* **90** 136
[14] Kanel G I, Razorenov S V, Bogatch A A and Grady D E 1996 *J. Appl. Phys.* **79** 8310
[15] Qi M L, Zhong S, He H L, Fan D and Zhao L 2013 *Chin. Phys.* B **22** 046203
[16] Trivedi P E, Asay J R, Gupta Y M and Field D P 2007 *J. Appl. Phys.* **102** 083513